

# Spot Welding Aluminum 6022-T4 to Galvanized DP600 sheet by Refill Friction Stir Spot Welding

Z. Shen<sup>1</sup>, J. Hou<sup>1</sup>, K. Chan<sup>2</sup>, N. Scotchmer<sup>2</sup>, N. Zhou<sup>1</sup>, A.P. Gerlich<sup>1</sup>

1. University of Waterloo, Mechanical and Mechatronics Engineering, Center for Advanced Materials Joining, Waterloo, Canada
2. Huys Industries Ltd., Toronto, Canada

## Abstract

Sheet metal welding in the automotive manufacturing industry is encountering increasing challenges while joining light weight alloys. For some time, resistance spot welding (RSW) has been the method of choice to join the vast array of automotive structural steels based on the speed and low cost; however, new combinations of non-ferrous materials suffer from limited weldability by RSW. Specifically, aluminum sheet metals offer many desirable properties for use in sub critical components such as body skins or brackets and latches, and advanced high strength steels are becoming commonplace for components requiring extremely high strength for rigidity and crashworthiness. However, joining these two dissimilar metals to each other presents a challenge for manufacturing. The present work examines Refill Friction Stir Spot Welding (RFSSW) to join aluminum sheet to zinc coated steel. Joints were made without melting of either of the base materials utilizing the plastic flow of the aluminum sheet to generate pressure and heat during welding. Weld parameter testing along with metallography including SEM/EDX analysis was performed to investigate the joining mechanism and define an operational window which can meet overlap shear fracture load requirements of AWS standards.

**Keywords:** *AL6022-T4, DP600, Refill Friction Stir Spot Weld, Dissimilar Joint*

## Introduction

With stringent government standards targeting reduced carbon emissions, vehicle light weighting in conjunction with engine downsizing is a popular solution to reduce emissions. As a result, there has been an increase in the application of light weight alloys in automotive structures to reduce overall mass of the vehicle. The use of aluminum and magnesium alloys for components such as body skins, brackets, sub-frames and latches, coupled with advanced high strength steel (AHSS) for structural components are becoming commonplace. Traditionally, resistance spot welding (RSW) has been the prime choice for joining automotive sheet metals;

however, RSW can no longer effectively produce structurally sound joints with the introduction of incompatible and novel material combinations due to their physical and chemical properties, especially the differences in melting temperatures and mutual solubility. Additionally, severe heating and cooling cycles from fusion welding can cause weld defects such as cracking, porosity, and bulk intermetallic compound (IMCs) formations, many of which are detrimental to weld integrity and strength [1, 2]. This motivates the application of solid state joining technologies, such as friction welding [3], ultrasonic spot welding [4], friction stir welding [5], as well as friction stir spot welding to be potential to replacement of resistance spot welding (fusion welding) in joining these combinations of non-ferrous and ferrous materials [6]. The main advantage of solid state joining technology is minimized energy input, which limits the formation of bulk IMCs, thermal distortion and residual stresses [7].

The present study focuses on the application of refill friction stir spot welding (RFSSW). This process was developed by Helmholtz-Zentrum Geesthacht in Germany in 1999 to achieve a larger effective bonded region and higher weld strength compared to conventional FSSW (without the refill capability) [8]. In conventional FSSW, a single piece tool (with only a cylindrical should and pin feature) is only plunged and retracted from the sheets in two steps. In contrast, RFSSW uses a tool with multiple pieces in four steps, summarized in Figure 1. In the first stage shown in Figure 1a, the tool used in RFSSW comprises a stationary clamp ring, an external sleeve and an internal pin. The role of the clamping ring is to hold the workpieces firmly in contact during the welding process, and prevent the sheets from lifting and separating as the plasticized material is displaced by the pin and sleeve. The sleeve and pin rotate together while able to advance and retract independently, operated by servo-actuators. The joint forms by plasticizing, and displacing the material in a process similar to back extrusion, and the refill FSSW process can be divided into two variants (pin plunge variant and sleeve plunge variant). So far, the sleeve plunge variant is the most commonly used variant, since it produces a larger effective welded area, but this variant demands higher plunge force [9]. The sleeve variant RFSSW process is schematically shown in Figure 1a-d, which has already been described in detail in the prior literatures [10, 11, 12].

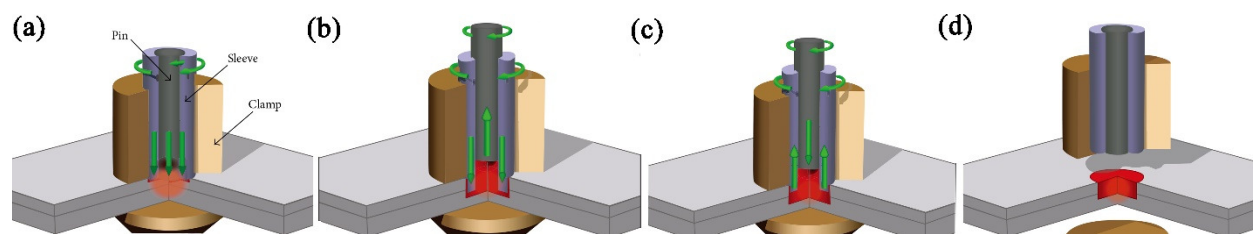


Figure 1: Schematic of the Refill Friction Stir Spot Welding Process (Sleeve Plunge Variant)

Tool wear in conventional non-refill FSSW is reportedly much more excessive compared to that in linear FSW since wear mainly occurs in the tool plunge period [13], however 100,000 welds can still be achieved without degradation in joint strength in aluminum sheet welds [14]. For dissimilar metal joints in RFSSW, in order to obtain mechanical interlocking by displacing the

bottom ferrous material into the upper lightweight material sheet, it is necessary to plunge the tool pin into the bottom sheet. This would require an advanced tool material, such as W–25 wt-%Re or WC-Co to be used [6, 15]; however, such materials are not currently available for RFSSW tooling. Previous research has shown that acceptable joint strengths can be achieved by purely metallurgical or diffusion bonding mechanisms, with the lightweight alloy sheets set as the top sheet when joining to a harder material. In this case, the tool plunge depth could be carefully controlled to avoid direct contact of the tool into the bottom steels, making it possible to use a tool made of common tool steels, and maintains the flat interface profile between the sheets [16, 17, 18, 19, 20, 21]. In these cases, the tool penetration depth is the most influential factor for weld integrity and strength. For example, Lee et al. [19] found that the weld strength increased with increasing tool penetration in the top Al alloy, but excessive tool penetration caused defects and deformation of the top Al alloy sheet. The presence of a zinc coating on galvanized steel surface can promote the formation of Al–Zn or Mg–Zn eutectic structure at the interface, which is believed to be beneficial to the bonding formation and weld strength. Ibrahim et al. [20] reported that Zn coating was melted or softened and circumferentially re-solidified around the nugget, and IMCs were formed along the interface resulting in the joining of Al or Mg to steel. Al/steel weld showed poor fatigue strength since circumferentially re-solidified Zn brought about the stress relaxation at the edge of the Al/galvanized steel nugget. Shen et al. [17] found the static and fatigue performance of Mg/steel dissimilar refill friction stir spot weld can be enhanced by the brazing around the weld boundary, and the brazing effect was derived from the zinc coating on the steel surface.

The present study focused on the investigation of aluminum to galvanized steel sheet dissimilar RFSSW welds. Optimization of welding parameters, and evaluation of interfacial bonding, thermal cycle and mechanical properties, was performed to evaluate the role of tool temperature. This preliminary research serves as a starting point for further optimization of parameters to maximize joint strength in tools with supplemental cooling.

## Experimental Procedure

### Materials

The base materials used for the present study are 1.6mm thick AA6022-T4 (top sheet) and 2.0mm galvanized (zinc coated) DP600 steel sheets (bottom sheet). Table 1 summarizes the chemical composition of the sheet metals used.

Table 1: Material Chemical Composition

Mat	Thickness [mm]	Coating		Base Metal, wt-%							
		Al	Cr	Cu	Mg	Mn	Si	Ti	Zn	Fe	
AA6022-T4	1.6	None	Remainder	0.1	0.01-0.11	0.45-0.070	0.02-0.10	0.80-1.5	<0.15	<0.25	0.05-0.20
				Fe	C	Mn	Si	P	S	Cr+Mo+Ni	
DP600	2	GI	Remainder	0.14	2	1.5	0.04	0.015	1		

Characterization of the galvanized DP600 sheets was performed to examine the zinc coating thickness, which was found to be an average of 6.5  $\mu\text{m}$ . The measured coating thickness is considered very thin and can be easily disturbed by the stirring action of the welding process, hence additional consideration of welding parameter selection was taken into account. The AA6022 and DP600 steel coupons were cleaned with ethanol before the welding process. Test specimens were fabricated with two 30mm $\times$ 100mm coupons overlapped by 30mm, and the welds were made at the center of the overlapped area according to the American Welding Society (AWS) standard D 17.2 [22].

### **Welding Setup**

The welding in the present study was conducted using a Harms & Wende RPS100 refill friction stir spot welding machine. The system consists of the 3-piece weld tool; the stationary clamping ring and a pair of rotating and vertical shifting sleeve and pin. The diameter of the clamp ring, sleeve and pin are 15, 9 and 6 mm, respectively. The welding process sequences consists a combination of tool rotation and penetration depth as well as a series of sequence timings; pre-heat, plunge, dwell, retract, and post heating dwell time. Depending on the contribution of parameters towards energy input at the weld interface, ultimately controlling the corresponding weld performance. Two main welding parameters, plunge depth and dwell time, were found to be particular influential to weld strength for dissimilar welding. As such, these two parameters varied, while the remaining control parameters were constant. The welding parameters used are summarized in Table 2

*Table 2: Weld Schedule Selection Matrix*

<b>Welding Parameter Selection Matrix</b>	
Spindle Rotation Speed [RPM]:	1800
Surface Friction Dwell Time [s]	0.5
Plunge Time [s]	0.207
Plunge Depth [mm]	0.8-1.4 (50-87.5% sheet thickness)
Stirring Dwell Time [s]	1, 2, 3
Tool Retract Time [s]	0.5
Surface Dwell Time After Retraction [s]	0.25

### **Temperature Measurement Setup**

Preliminary welding trials of AA6022 to DP600 indicated that high welding temperatures (energy input) resulting from both high plunge depth (95% aluminum sheet thickness) and long dwell time (>3 seconds) resulted in low strength or negligible bonding. Two explanations account for the unbonded conditions with the particular welding parameters: excessive disturbance of the zinc coating from physical stirring, and excessive heating of the interface. High weld interface temperatures, specifically beyond the 94% Zn-Al eutectic point of 381 $^{\circ}\text{C}$  (based on the binary phase diagram [23]), can result in zinc liquidation and oxidation, leading to poor weld strength. As a result, the tool and weld interface temperature control was of high importance for this study.

In order to better control tool temperature for sequential welding, a prototype water cooled copper cooling block was fabricated and attached to the outer surface of the clamping ring tool. The cooling block was used concurrently with the standard tool cooling circuit, which employs a thin copper conductive cooling sleeve in the clamp. Thermal measurements of the tool clamp were acquired by welding a K-type thermocouple to the outer boundary of the clamp ring as indicated in Figure 2a and b, at a location 5mm away from the end of the tool. The interface temperature acquired by sandwiching a thin K-type thermocouple within a machined out groove between the weld interface Figure 2c. Thermal measurements were acquired with National Instruments 9213 DAQ system.

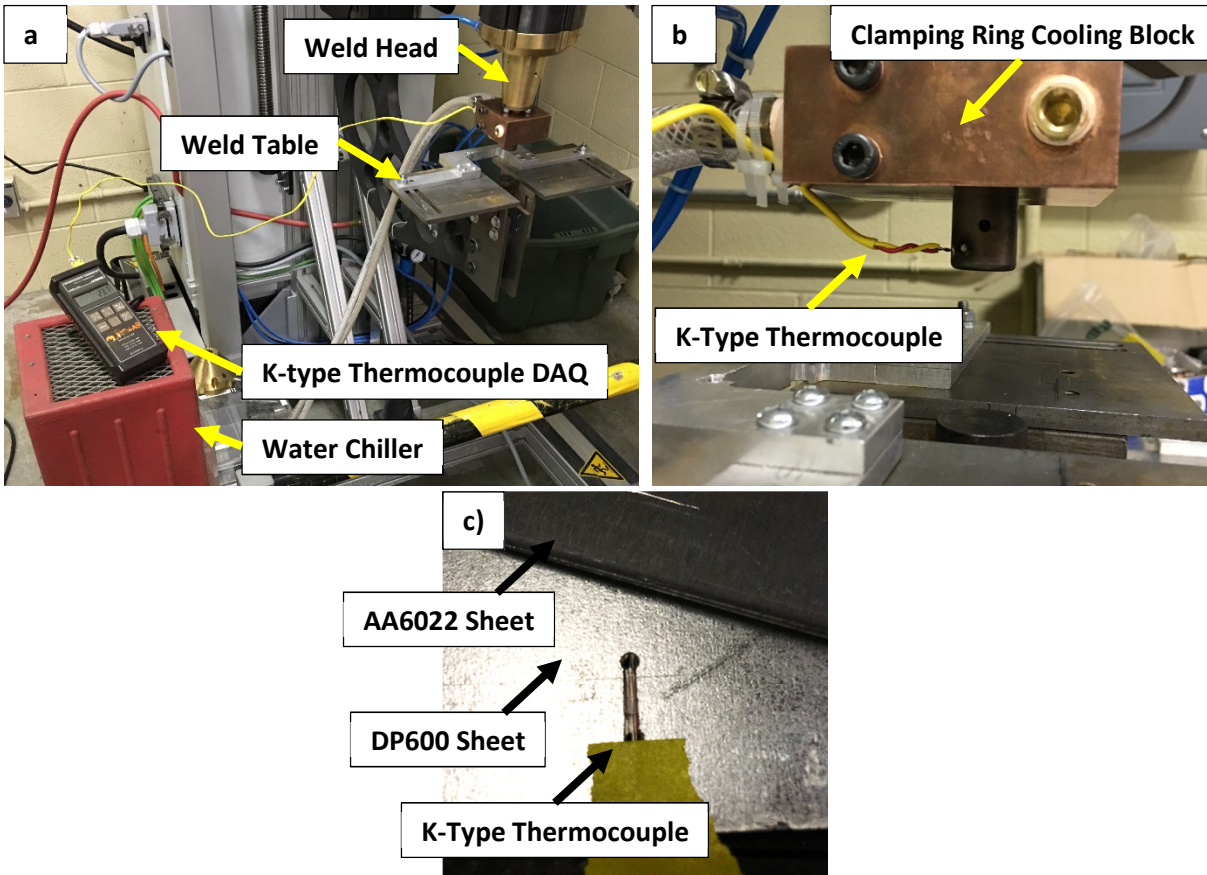


Figure 2: Spot welder setup: a) external tool shoulder cooling circuit and temperature acquisition setup, b) tool shoulder cooling block and thermocouple setup and, c) thermocouple placement within grooved out steel plate

### **Tensile Testing Setup**

Tensile testing was performed in lap-shear setup with a constant cross head speed of  $10\text{mm min}^{-1}$ , as recommended by AWS D8.2M:2007 standard [24]. All tensile coupons were cut to  $30\times 100\text{mm}$  with the rolling direction parallel to the longer side and the weld situated in the center of  $30\times 30\text{mm}$  overlapped region (Figure 3). Since the weaker material for the weld combination is the AA6022-T4 material, the minimum required shear strength was calculated based on the AWS standards, as  $3.87\text{kN}$  [24].

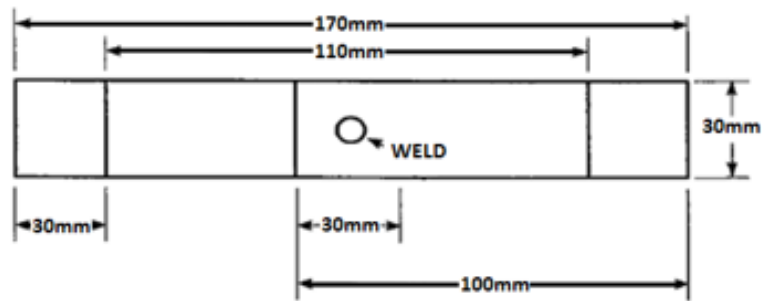


Figure 3: Weld specimen setup for tensile lap shear testing and characterization

### **Characterization Setup**

The welds are sectioned through the weld center, and prepared using standard metallographic techniques with a final polishing with 3 $\mu$ m diamond. The microstructure characterization and chemical analysis were conducted by using a JEOL JSM-6460 scanning electron microscope (SEM) operated at 20kV accelerating voltage equipped with an ENCA 3.5 energy dispersive X-ray (EDX) analysis system. The lap shear tensile tests were performed at a rate of 10mm/min by using a Tinius Olsen (H10KT) tensile testing machine. All of the strength values were obtained by averaging the strengths of three individual specimens made at the same welding condition.

## **Results and Discussions**

### **Parameter Optimization and Tensile Properties**

Each combination of welding schedule summarized in Table 2 was welded with three repetitions and tensile tested for weld strength. Figure 4 illustrates the all of the weld strengths against recorded maximum tool temperatures of each weld, separated with three different dwell times regardless of different plunge depths. It should be noted each weld was conducted at a similar starting temperature of 55  $\pm$  5 $^{\circ}$ C for weld consistency. Welds performed with 1s dwell time resulted in fracture strengths mainly from 2.5 to 4kN, with a few exceptions reaching to 5kN. As the dwell time increases from 2s to 3s, the maximum tool temperature recorded increases as well. When a 2s dwell time is applied the welds performed much better, with more welds exceeding the minimum requirement of 3.87 kN [24]. When a 3s dwell time is applied, the welds performed with strengths capable reaching as high as 6.23kN. However, when the tool temperatures during welding approach 350 $^{\circ}$ C, the weld strength plummets well below the minimum requirement.

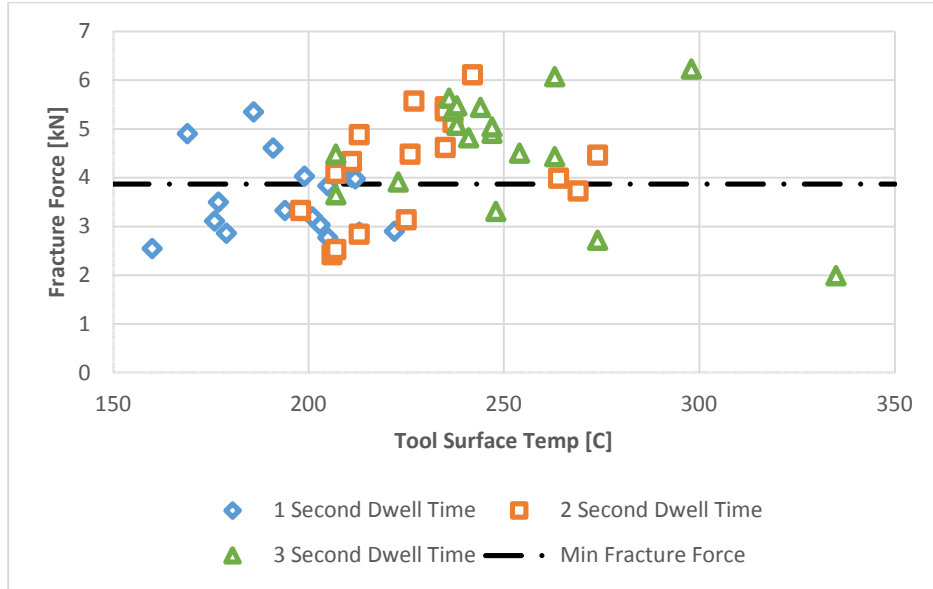


Figure 4: Weld Parameter Optimization Plots: a) tool temperature to weld strength influence plot and

Three representative welds based on tooling temperature, designated as insufficient, acceptable, and overheated welds, were selected from the weld parameter matrix. Weld strengths and clamping ring maximum temperatures for each representative welds are summarized in Table 3. As previously noted, the integrity of the welds is governed by the temperature and energy input from the weld schedules. With insufficient energy input, the maximum tool temperature reached was 179°C and the weld strength achieved was below the minimal requirement of 3.87kN. With sufficient energy input, the weld strengths exceed and nearly doubles the minimal required strength, while the tool temperature reaches 298°C. Finally, when overheating occurs with an overshoot of energy input, tool temperatures reach 335°C and the weld strengths plunge below acceptable levels.

Table 3: Representative weld parameter data

Condition	Insufficient	Sufficient	Overheated
Dwell Time [s]	1	3	3
Plunge Depth [mm]	0.8	1	1.4
Repetition	Fracture Force [kN]		
1	2.86	5.09	3.31
2	3.11	5.37	1.99
3	2.55	6.23	2.72
Average	2.84	5.56	2.67
Max Tool Temp	179	298	335

Each weld condition produces distinct appearances when observing weld fracture interfaces (Figure 5). When sufficient energy is provided, the weld interface presents with a combination of a white and grey ring appearance Figure 5a. The white artifact in the weld center occurs when the welds are subjected to high temperatures, while the grey artifact is a result of zinc IMCs with

the aluminum. Due to the nature of zinc coating during the welding process, a large amount of zinc coating migrates towards the weld center as the sleeve plunges into the aluminum sheet. During the sleeve plunging process, a slight imbalance of temperature present within the weld interface between the pin and sleeve area. The upper layer of zinc experiences high temperature from the stirring effect from the sleeve and migrates towards the weld center, while the bottom layer of zinc experiences sufficient temperatures to begin brazing or possibly diffusion bonding. When insufficient energy is provided to the weld, diffusion bonding does not happen between zinc and aluminum. As a result, the weld interface has a shiny aluminum appearance as shown in Figure 5b. At the other extreme, when too much energy is applied, the entire weld interface appearance of the fracture surface is almost entirely white Figure 5c.

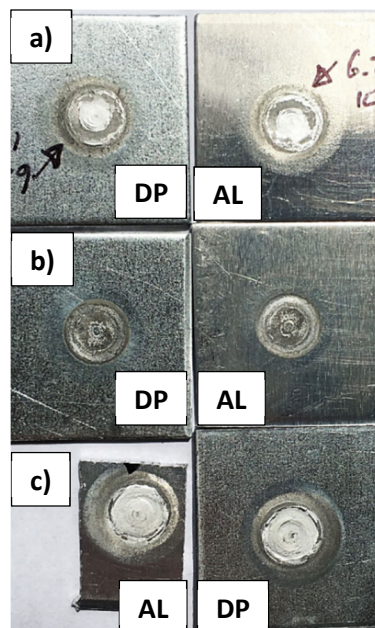


Figure 5: Fracture Interface Appearance: a) Optimal Heat (6.23kN @ 298°C), b) Insufficient Heat (2.86kN @ 179°C), and c) Overheated (1.99kN @ 335°C)

### **Optical and Scanning Electron Microscopy**

Figure 6a and b reveal the weld surface appearance and optical macrostructure of the weld made with acceptable energy input welding conditions, involving 1800RPM summarized in Table 3. The weld surface appears shiny and uniform with the original workpiece surface. As shown in Figure 6a, an annular indent imposed by the clamp ring was formed around the weld, which is slightly past the weld surface. As indicated in below Figure 6b, the weld boundary was marked by black lines, and voids can be observed within the weld boundary. The Al/steel interface is comparatively uniform, no macro-scale plastic deformation can be observed, and the top aluminum alloy sheet was imposed onto the bottom DP steel sheet by the welding tool. However, micro-scale cracking was noted at the Al/steel interface. The current study does not



provide the microstructure details of the top Al sheet, since the previous research showed that the upper sheet microstructure scarcely affects the weld strength when interfacial fracture dominates [15, 16].

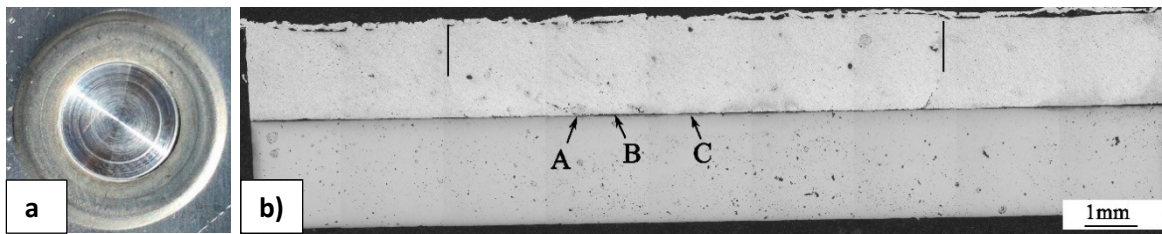


Figure 6: Optical Micrographs of Al-DP Welds: a) Weld surface appearance and b) Weld cross-section produced using 1800 RPM, 1.0mm penetration, and a 3s dwell time

Figure 7a-c illustrates SEM micrographs at locations A and C indicated in Figure 6b. As illustrated in these figures, the zinc coating thickness distribution is not uniform, ranging from 0.5 to 3.2  $\mu\text{m}$  at locations A and B, and around 20 $\mu\text{m}$  at the weld center in Location C. It can be observed that the zinc coating under the sleeve shifted into the weld center due to a cylindrical cavity that was created during the sleeve plunge and pin retreat phase. Furthermore, the bonding has occurred under the sleeve before the sleeve moves upward and pin moves downward, which promoted displaced zinc coating to be entrapped in the weld center. As shown in Figure 7a, cracking can be observed at the boundary of sleeve and pin, whose direction is consistent with the material flow. The chemical compositions in the locations A-F were quantified in Table 4, where the zinc content ranged from 16.9 to 19.5%, and the iron content ranged from 0.5% to 2.9%. Meanwhile, cracking can be observed in Figure 7b. The chemical compositions in locations of (i) through (vii) were quantified in Table 4 where the zinc content ranged from 18.6% to 24.3%, and the iron content ranged from 0.8% to 2.3%. It can be concluded that the zinc penetrated into the top Al alloys along the grain boundary, which is caused by high temperature and upward motion of material flow imposed by the tool. As noted previously [23], Al-Zn low melting point eutectic structure could be formed at the temperature of 351°C, and the maximum tool temperature reaches 335°C (see Figure 4). Prior work by Suhuddin et al. and Shen et al. showed the maximum temperature can reach 450°C and 501°C, respectively [12, 25], which readily explains the formation of Al-Zn eutectic structure. It also can be believed that IMCs of Al-Fe also can be formed in these locations, which has been confirmed by Chen et al. that continuous layer of  $\text{FeAl}_2$  particles, which appeared to originate from the zinc coating on the DP600 steel surface [16].

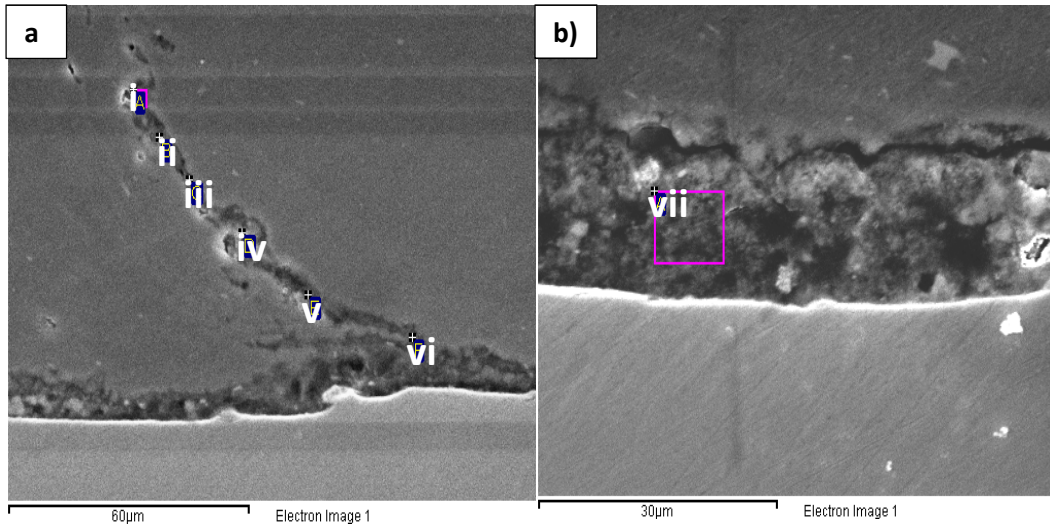


Figure 7: SEM Micrographs of locations (a) A and (b) location C in Figure 6b.

Table 4: EDX Chemical Composition Quantification Results (wt%) indicated in Figure 7.

Spectrum	Al	Fe	Zn	Total
i	82.2	0.5	17.3	100
ii	81.5	0.8	17.7	100
iii	82.4	0.7	16.9	100
iv	79.0	1.6	19.4	100
v	77.6	2.9	19.5	100
vi	80.1	2.3	17.6	100
vii	73.4	2.3	24.3	100

## **Thermal Studies of AA6022-T6 to DP600 Dissimilar RFSSW Welds**

### **Consecutive Welding Trials – Additional Cooled VS Stock Cooling**

The high tendency for tool overheating observed during the preliminary trials in this study suggests that control of the tool temperature is critical for the process to be used in an industrial setting. As a result, an additional cooling collar was fabricated and attached to the clamping ring in order to improve heat extraction and prevent overheating and weld separation as discussed earlier. A comparison of the standard cooled and externally cooled clamping ring was conducted to test the stability of the weld strengths in sequential welding. Welds were made with a satisfactory welding schedule summarized in Table 3. Figure 8 summarizes the comparison data between stock cooling (Figure 8a) and additional cooling (Figure 8b) trials. The welds were conducted at 10s intervals to allow for constant cooling time between welds, which is the most practical repetition speed achievable in manually repeated experiments. The welds with the

additional cooling heatsink on the tool clamp outperform the standard cooled tooling welds by a margin of only 3 consecutive welds; however, the overall weld strengths of the additionally cooled case were much higher by an average difference of 2.24kN. Weld strengths tended to increase for the first 5 welds for both cases. While the maximum weld strength peaked at 6.32kN for the 5<sup>th</sup> weld using the standard tooling, the weld strength continued to increase for the additionally cooled tool, peaking at 7kN for the 7<sup>th</sup> weld. It can be noted that in both scenarios, the weld force drastically decreased once the tool temperature reaches 350°C and subsequent welds at higher tool temperatures, and failed to produce suitable welds.

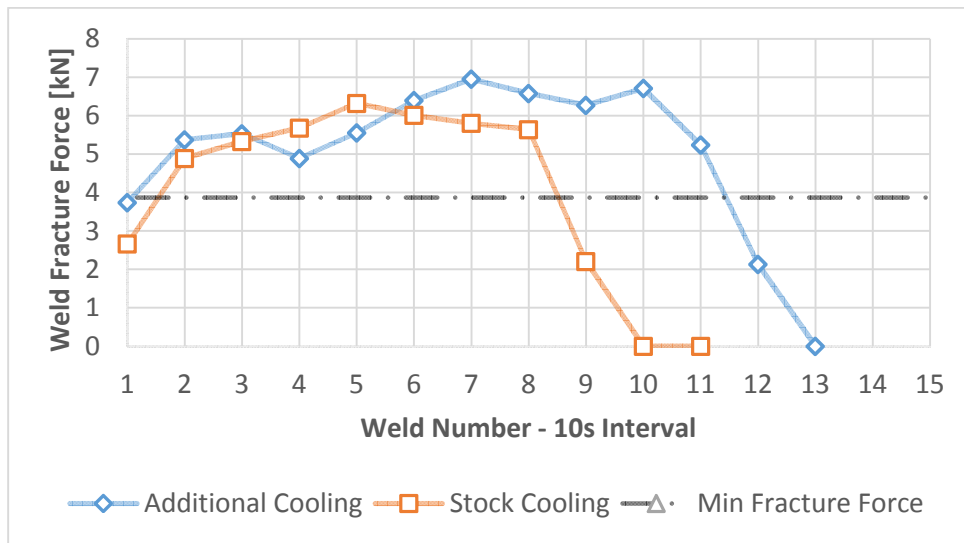


Figure 8: Overlap fracture load measurements for consecutive welding trials with and without additional cooling.

## Interface Temperature Measurement

Based on the thermal and weld strength results in the consecutive welding trials, a large window of acceptable tool temperatures exist between the first weld to the breaking point at 350°C. With each subsequent weld, the pre-weld temperature of the tool increased up to the critical temperature where satisfactory welds are no longer achievable. It can be assumed that the temperature at the weld interface would be much greater than the tool surface temperature. This raises the question of the correlation between the specific weld interface temperatures at different pre-weld temperatures of the tool, and how this would affect weld strength. For example, the thermal profile of a subsequent weld, when a 150°C pre-heat was applied to the tool is illustrated in Figure 9. The preheat energy was applied using a previous weld cycle. The peak weld interface temperature reached 389°C, just below the 94% Zn-Al eutectic temperature, while the maximum tool temperature reached 216°C. The final weld strength is thought to be based on the formation of the Zn-Al eutectic, however the peak temperature and pre-heat temperature relation is not fully characterized. Based on the thermal and weld strength results in the consecutive welding trials, a window of acceptable weld strength is available between the first weld up to the breaking point at a tool temperature of 350°C. The interfacial temperature measurement trials were conducted with the 1mm plunge and 3s dwell weld parameter.

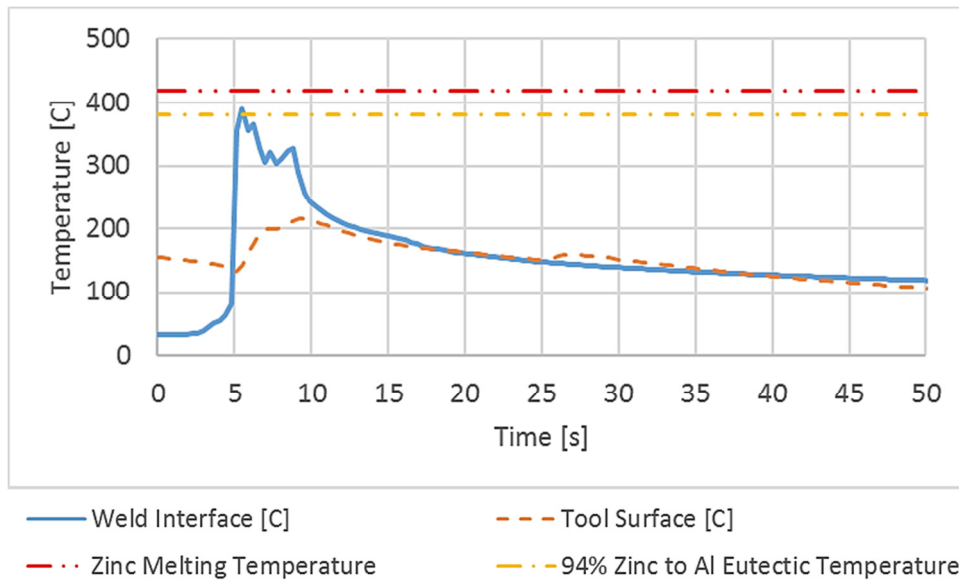


Figure 9: Interface Thermal Profiles of Al/DP Dissimilar RFSSW with 150°C Tooling Preheat.

## Summary

Refill friction stir spot welding of aluminum to zinc-coated dual phase steel was possible with a maximum overlap shear strength of 7kN. However, repeated consecutive welds suffered from a loss of weld strength when a critical tool temperature was reached. The correlation between tool pre-weld temperature and weld strength was unclear, however can be related to the formation of Al-Zn eutectics. Satisfactory sequential welds were made and would increase in strength up to a critical temperature of the weld tool, after which joint strength dropped suddenly. The use of an external cooling block provided an increase in the number of welds achievable before overheating occurred during consecutive welding with a 10 sec cooling time between welds. The overall weld strength achievable was slightly improved with the application of additional cooling, suggesting that improvements can be made using further optimized tool designs which would be able to maintain more stable temperatures and avoid exceeding critical temperatures at the interface.

## Acknowledgments

This work has been supported by the Natural Science and Engineering Council (NSERC) of Canada, the Canadian Foundation for Innovation. Additional support from Kevin Chan, at Huys Industry is greatly appreciated for providing tool cooling blocks used for this study.

## References

- [1] K. Miyamoto, S. Nakagawa, C. Sugi, H. Sakurai and A. Hirose, "Dissimilar joining of aluminium alloy and steel by resistance spot welding," *SAE International Journal of Materials and Manufacturing*, vol. 2, no. 01-0034, pp. 58-67, 2009.
- [2] L. Agudo, D. Evidi, C. H. Schmaranzer, E. Arenholz, N. Jank, J. Bruckner and A. R. Pyzalla, "Intermetallic Fe x Al  $\gamma$ -phases in a steel/Al-alloy fusion weld.," *Journal of materials science*, vol. 42, no. 12, pp. 4205-4214, 2007.
- [3] M. Yilmaz, M. Col and M. Acet., "Interfaces properties of aluminium/steel friction-welded components," *Materials Characterization*, vol. 49, no. 5, pp. 421-429, 2002.
- [4] F. Haddadi, D. Strong and P. B. Prangnell, "Effect of zinc coatings on joint properties and interfacial reaction in aluminium to steel ultrasonic spot welding," *JOM*, vol. 64, no. 3, pp. 407-413, 2012.
- [5] T. DebRoy and H. K. D. H. Bhadeshia, "Friction stir welding of dissimilar alloys - a perspective," *Science and Technology of Welding & Joining*, 2013.
- [6] T. Liyanage, J. Kilbourne, A. P. Gerlich and T. H. North, "Joint formation in dissimilar Al alloy/steel and Mg alloy/steel friction stir spot welds," *Science and Technology of Welding and Joining*, vol. 14, no. 6, pp. 500-508, 2009.
- [7] Z. Shen, Y. Chen, M. Haghshenas and A. P. Gerlich, "Role of welding parameters and interfacial bonding in dissimilar steel/aluminium friction stir welds," *Engineering Science and Technology, an International Journal*, vol. 18, no. 2, pp. 270-277, 2015.
- [8] C. Shilling and J. d. Santos. Washington DC: U.S. Patent and Trademark Office Patent 6,722,556, 2004.
- [9] S. T. Amancio-Filho, A. P. Camillo, L. Bergmann, J. F. D. Santos, S. E. Kury and N. G. Machado, "Preliminary investigation of the microstructure and mechanical behaviour of 2024 aluminium alloy friction spot welds," *Materials Transactions*, vol. 52, no. 5, pp. 985-991, 2011.
- [10] T. Rosendo, B. Parra, M. A. D. Tier, A. A. M. D. Silva, J. F. D. Santos, T. R. Strohaecker and N. G. Alcantara, "Mechanical and microstructural investigation of friction spot welded AA6181-T4 aluminium alloy," *Materials & Design*, vol. 32, no. 3, pp. 1094-1100, 2011.
- [11] Z. Shen, X. Yang, Z. Zhang, L. Cui and T. Li, "Microstructure and failure mechanisms of refill friction stir spot welded 7075-T6 aluminium alloy joints," *Materials & Design*, vol. 44, pp. 476-486, 2013.
- [12] Z. Shen, Y. Chen, J. S. C. Hou and A. P. Gerlich, "Influence of processing parameters on microstructure and mechanical performance of refill friction stir spot welded 7075-T6 Aluminium Alloy," *Science and Technology of Welding and Joining*, vol. 20, no. 1, pp. 48-57, 2015.
- [13] T. J. Lienert, J. W. L. Stellwag, B. B. Grimmer and R. W. Warke, "Friction stir welding studies on mild steel," *Welding Journal - New York*, vol. 82, no. 1, pp. 1-5, 2003.
- [14] J. Hinrichs, C. Smith, B. Orsini, R. DeGeorge, B. Smale and P. Ruehl, "Friction Stir Welding for the 21st Century Automotive Industry," in *155th FSW Symposium*, Waukesha, WI USA.
- [15] A. A. M. D. Silva, E. Aldanondo, P. Alvarez, E. Arruti and A. Echeverria, "Friction stir spot welding of AA 1050 Al alloy and hot stamped boron steel (22MnB5)," *Science and Technology of Welding and Joining*, 2013.
- [16] Y. Chen, J. Chen, B. S. Amirkhiz, M. J. Worswick and A. P. Gerlich, "Microstructures and properties of Mg alloy/DP600 steel dissimilar refill friction stir spot welds," *Science and Technology of Welding and Joining*, vol. 20, no. 6, pp. 494-501, 2015.
- [17] Z. Shen, Y. Ding, J. Chen and A. P. Gerlich, "Comparison of fatigue behaviour in Mg/Mg similar and Mg/steel

dissimilar refill friction stir spot welds," *International Journal of Fatigue*, vol. 92, pp. 78-86, 2016.

- [18] Y. Uematsu, T. Kakiuchi, Y. Tozaki and H. Kojin, "Comparative study of fatigue behaviour in dissimilar Al alloy/steel and Mg alloy/steel friction stir spot welds fabricated by scroll grooved tool without probe," *Science and Technology of Welding and Joining*, vol. 17, no. 5, pp. 348-356, 2012.
- [19] Y. C. Lee, D. H. Choi, Y. M. Yeon and S. B. Jung, "dissimilar friction stir spot welding of low carbon steel and Al-Mg alloy by formation of IMCs," *Science and Technology of Welding and Joining*, 2013.
- [20] I. Ibrahim, Y. Uematsu, T. Kakiuchi, Y. Tozaki and Y. Mizutani, "Fatigue behaviour of dissimilar Al alloy/galvanized steel friction stir spot welds fabricated by scroll grooved tool without probe," *Science and Technology of Welding and Joining*, vol. 20, no. 8, pp. 670-678, 2015.
- [21] E. Fereiduni, M. Movahedi and A. H. Kokabi, "Dissimilar Al/steel friction stir spot welding: To penetrate into lower steel sheet or not?," *Science and Technology of Welding and Joining*, pp. 1-7, 2016.
- [22] American Welding Society, AWS D17.2 Specification for resistance welding for aerospace applications, AWS, 2007.
- [23] ASM International, "Al (Aluminium) Binary Alloy Phase Diagram," in *ASM Handbook Volume 3 - Alloy Phase Diagrams.*, ASM International, 1992, pp. 2.4-2.56.
- [24] A. D. C. o. A. Welding, AWS D81M:2007 Specification for Automotive Weld Quality - Resistance Spot Welding of Steel, Miami, FL: American Welding Society, 2007.
- [25] U. F. H. F. V. & D. S. J. F. Suhuddin, "The thermal cycle during the dissimilar friction spot welding of aluminum and magnesium alloy," *Scripta Materialia*, vol. 68, pp. 87-90, 2013.